Energy Conversion and Management 277 (2023) 116670

Contents lists available at ScienceDirect

Energy Conversion and Management

journal homepage: www.elsevier.com/locate/enconman

Techno-economic evaluation of hydrogen and ammonia as energy carriers in a multi-generation system

Du Wen [a,b,*], Shicheng Liu [c], Zhiyuan Ning [c], Muhammad Aziz [b,*]

[a] Department of Mechanical Engineering, The University of Tokyo, 7-3-1 Hongo, Bunkyo-ku, Tokyo 113-8656, Japan
[b] Institute of Industrial Science, The University of Tokyo, 4-6-1 Komaba, Meguro-ku, Tokyo 153-8505, Japan
[c] State Key Laboratory of Multiphase Flow in Power Engineering, Xi'an Jiaotong University, Xi'an 710049, China

ARTICLE INFO

Keywords:
Carbon neutrality
Energy storage
Hydrogen and ammonia
Optimal planning

ABSTRACT

Green hydrogen is suitable for grid-scale energy storage to increase the penetration of renewable energy, and it is also an alternative to fossil fuels. However, it still suffers from storage problems owing to its low volumetric energy density, embrittlement, and very low boiling point. To improve safety and reduce cost, green ammonia has been proposed as a substitute for hydrogen and has attracted considerable attention. In this study, a multi-generation system was proposed to compare green hydrogen and green ammonia as energy carriers. Four scenarios are discussed and the performances under different energy carriers, constant and time-of-use electricity prices, and on-grid and off-grid operations are compared. The optimal planning of the system was formulated as a mixed-integer linear programming problem and was evaluated using supply and demand profiles hourly over a year. The objective was to maximize profitability, which is reflected by the cumulative cash position and payback period. The results revealed that the hydrogen-based system was superior to the ammonia-based system. In the hydrogen-based scenario, the cumulative cash position was 83.43 MUSD and the payback period was 14 years. The cumulative cash position and payback period were 12.78 MUSD and 22 years, respectively, in the ammonia-based scenario. To improve profitability, it is recommended to increase the capacity for hydrogen/ammonia production and reduce the capacity for backup power generation.

1. Introduction

Since signing the Paris Agreement in 2016, several countries have included carbon neutrality on the agenda, pledged to achieve it by 2050, and proposed relevant policies, regulations, and schemes. Currently, the efforts are focused on the energy sector, which contributes to the highest carbon emissions. Promoting further electrification and expanding the penetration of renewable energy have been identified as the most promising solutions for achieving low-carbon emissions in the energy sector. However, the intermittent nature of renewable energy is the main difficulty faced by grids that are not designed for renewable energy. Energy storage technologies have attracted considerable attention as a solution to this problem; however, not all of them are suitable for grids in terms of technical and economic aspects. Green hydrogen is suitable for bulk energy storage because of its high gravimetric energy density, favorable cradle-to-grave characteristics, and lack of carbon emissions during power generation [1]. In addition to energy storage, it has versatile applications. For example, it can replace coke as a reducing agent in the iron industry; it is an important feedstock in chemical production and a clean fuel. Moreover, the existing natural gas infrastructure is compatible with hydrogen and hence requires less investment for upgrading. Considering the global energy crisis and depletion of fossil fuel reservoirs, alternative fuels are urgently required to ensure energy security, as the predictions from different institutes have revealed that the production of oil is approaching or has already reached its peak. Therefore, researchers have envisioned a hydrogen economy [2] in which green hydrogen, produced using water electrolysis based on renewable energy, is not only used in the electricity and heat sectors but also in the industry and transportation sectors, which are difficult to

Abbreviations: AS, Ammonia synthesis; CAPEX, Capital expenditure; CCP, Cumulative cash position; EMS, Energy management system; MILP, Mixed integer linear programming; MUSD, Million U.S. dollar; OPEX, Operational expenditure; PBP, Payback period; PV, Solar photovoltaic; SoC, State of charge; SOEL, Solid oxide water electrolysis; SOFC, Solid oxide fuel cell; SOFCA, Ammonia based SOFC; SOFCH, Hydrogen based SOFC; STA, Ammonia storage tank; STH, Hydrogen storage tank; WT, wind turbine.

* Corresponding authors.
E-mail addresses: wendu@g.ecc.u-tokyo.ac.jp (D. Wen), maziz@iis.u-tokyo.ac.jp (M. Aziz).

https://doi.org/10.1016/j.enconman.2023.116670
Received 8 July 2022; Received in revised form 5 January 2023; Accepted 6 January 2023
Available online 12 January 2023

Nomenclature

Symbols

$CAPEX$	CAPEX of the system, (USD)
$C_{\text{byproduct}}$	price of byproduct, (USD)
C^t_{ele}	electricity price at time t, (USD)
C_{H_2}	hydrogen price, (USD)
d_j	annual depreciation cost, (USD)
i	annual interest rate, (%)
$M_{\text{H}_2,\text{max}}$	maximum capacities of the hydrogen storage tank, (t)
$M_{\text{H}_2,\text{min}}$	minimum capacities of the hydrogen storage tank, (t)
$m^t_{\text{byproduct}}$	net production rate of byproduct, (kg·h^{-1})
$m^t_{\text{H}_2}$	net production rate of hydrogen, (kg·h^{-1})
$m^t_{\text{H}_2,\text{loss}}$	amount of hydrogen loss, (kg·h^{-1})
$m^t_{\text{H}_2,\text{SOEL}}$	hydrogen production rate of SOEL, (kg·h^{-1})
$\dot{m}_{\text{H}_2,\text{SOEL}}$	hydrogen production rate of SOEL in the simulation, (kg·h^{-1})
$m^t_{\text{H}_2,\text{SOFC}}$	hydrogen consumption rate of SOFC, (kg·h^{-1})
$\dot{m}_{\text{H}_2,\text{SOFC}}$	hydrogen consumption rate of SOFC in the simulation, (kg·h^{-1})
$m^t_{\text{H}_2,\text{sold}}$	amount of hydrogen sold to the market, (kg·h^{-1})
$m^t_{\text{H}_2,\text{sto}}$	amount of hydrogen storage at time t, (kg·h^{-1})
$m^{t-1}_{\text{H}_2,\text{sto}}$	amount of hydrogen storage at time t-1, (kg·h^{-1})
$m^t_{\text{NH}_3}$	net production rate of ammonia, (kg·h^{-1})
N_{PV}	installed number of solar cells, (–)
N_{WT}	number of wind turbines, (–)
n	system lifetime, (y)
$OPEX$	annual OPEX of the system, (USD)
$OPEX_t$	OPEX at time t, (USD)
$opex^t_{\text{es}}$	OPEX of the energy storage system, (USD)
$opex^t_{\text{hs}}$	OPEX of the hydrogen storage system, (USD)
$opex^t_{\text{rf}}$	OPEX of the renewable farm, (USD)
P^t_{AS}	output power of ammonia synthesis, (kW)
P^t_{as}	input power of the ammonia storage system, (kW)
P^t_{B}	input or output power of the battery, (kW)
$P_{\text{B,rated}}$	rated power of the battery, (kW)
P^t_{C}	output power of compression, (kW)
$\dot{P}_{\text{C}}$	output power of compression in the simulation, (kW)
P^t_{cell}	output power of a solar cell, (kW)
$P_{\text{cell,rated}}$	rated power of a solar cell, (kW)
P^t_{cur}	curtailment of renewable energy, (kW)
P^t_{demand}	electricity demand, (kW)
P^t_{es}	input or output power of the energy storage system, (kW)
P^t_{g}	imported electricity from the grid, (kW)
P^t_{hs}	power of the hydrogen storage system
P^t_{PV}	power of PVs, (kW)
P^t_{rf}	power of the renewable farm, (kW)
P^t_{SOEL}	power of SOEL, (kW)
$\dot{P}_{\text{SOEL}}$	power of SOEL in the simulation, (kW)
$P_{\text{SOEL,rated}}$	rated power of SOEL, (kW)
P^t_{SOFC}	power of SOFC, (kW)
$\dot{P}_{\text{SOFC}}$	power of SOFC in the simulation, (kW)
$P_{\text{SOFC,rated}}$	rated power of SOFC, (kW)
P^t_{turbine}	power of a wind turbine, (kW)
P^t_{WT}	power of wind turbines, (kW)
$P_{\text{WT,rated}}$	rated power of a wind turbine, (kW)
REV	annual revenue of the system, (USD)
REV_t	revenue at time t, (USD)
SoC_{max}	maximum SoC, (–)
SoC_{min}	minimum SoC, (–)
SoC_t	SoC of the battery, (–)
t	tax rate, (%)
v	wind speed, (m·s^{-1})
x_{SOEL}	binary variable, (–)
x_{SOFC}	binary variable, (–)

electrify and decarbonize. Thus, green hydrogen exhibits a cross-sector decarbonization potential. Several studies have been conducted on green hydrogen production [3], storage [4], and utilization [5] to progress towards a hydrogen-based economy.

However, hydrogen storage has some limitations in terms of cost and safety. Greater space and larger devices are required to achieve a lower volumetric energy density for the same unit of energy stored, which results in a cost penalty. It necessitates investments on safety precautions because the high flammability of hydrogen expedites its deflagration, and detecting the nearly invisible and smoke-free hydrogen flames is difficult. To counter the low volumetric density, high flammability, and energy loss of hydrogen storage [6], researchers have proposed other renewable synthetic fuels, such as ammonia [7], to replace hydrogen as an energy carrier. Ammonia has a high energy density and hydrogen content and is a zero-carbon fuel. It is also an important chemical widely used in fertilizers, acid gas removal, refrigerants, synthetic fibers, and explosives [8]. To use ammonia as a more efficient energy carrier, researchers have investigated ammonia-to-power technologies using electrochemical and thermochemical methods, including fuel cells [9], internal combustion engines [10], and gas turbines [11]. According to a report [12], ammonia is a cost-competitive fuel for heavy mining trucks and container ships.

Considering the advantages of green hydrogen/ammonia in attaining a low-carbon environment, particularly its cross-sector decarbonization potential, various multi-generation systems that use green hydrogen/ammonia as the energy carrier have been proposed and discussed in various studies. Thermodynamic analyses have been conducted on various hydrogen- and ammonia-based systems, which involve different green hydrogen/ammonia production, storage, and utilization techniques. Lutman et al. [13] proposed a sustainable multi-generation system based on solar and wind energy, which provides electricity, heating, cooling, and water desalination for remote areas. Both thermal energy and hydrogen storage units (water electrolysis and hydrogen combustor) were used to ensure continuous operation. The overall energy and exergy efficiencies were 50 % and 34 %, respectively. In [14], green hydrogen was directly used for ammonia synthesis (AS) in an ammonia-based system without storage, and ammonia-fed solid oxide fuel cells (SOFCs) were used to compensate for any electricity shortage. The system performance was evaluated hourly for a year via a dynamic simulation. The overall energy efficiency varied between 46.1 % and 53.3 %, whereas the overall exergy efficiency varied between 34 % and 41.5 %. Other studies have proposed multi-generation systems with different renewable energy sources [15], green hydrogen production methods [16], hydrogen[16]/ammonia[17] utilization methods, and system integration [18]. All of the studies mentioned above prove the technical feasibility of hydrogen- and ammonia-based systems.

A techno-economic analysis of a system using hydrogen or ammonia as energy carriers was conducted. Anand et al. [19] conducted a case study on an academic research building. A standalone hybrid renewable energy system equipped with hydrogen fuel cells and a battery bank was proposed to achieve 100 % renewable energy penetration at a cost of 0.203 USD·kWh^{-1}. A case study conducted on a university campus [20] investigated a grid-connected hybrid system consisting of photovoltaic (PV) cells, gas-fired trigeneration, and hydrogen production. The

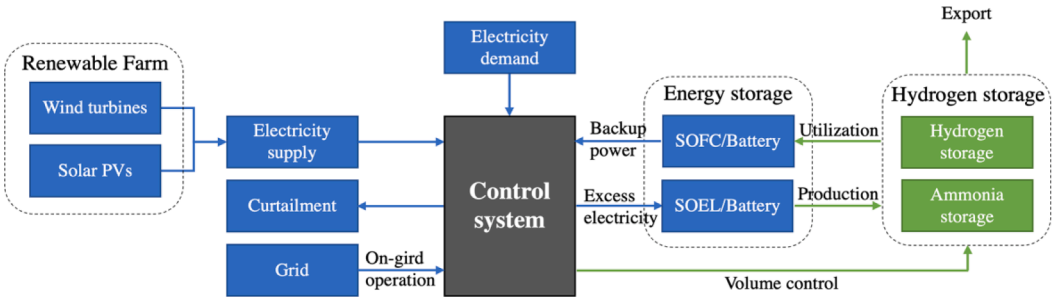

Fig. 1. Schematic of the integrated renewable multi-generation system.

Table 1
Description of scenarios involved in this study.

Name	Energy carrier	Electricity price	Electricity import	Grid connection
S1	Hydrogen	Constant	Not allow	Off-grid
S2	Hydrogen	Time of use	Not allow	Off-grid
S3	Hydrogen	Time of use	Allow	On-grid
S4	Ammonia	Time of use	Allow	On-grid

levelized cost of electricity in different scenarios was in the range of 0.061–0.065 USD·kWh^{-1}. Carlos et al. [21] conducted a techno-economic assessment of blue and green ammonia as energy carriers. Blue ammonia was produced by a gas-switching reforming plant fed by natural gas and an AS loop, whereas green ammonia was produced by a water electrolysis facility powered by renewable energy and an AS loop. Ammonia only served as a product. The levelized cost of ammonia showed that blue ammonia was cost-competitive.

The size and operation of an energy system significantly affect profitability; therefore, several researchers have not only focused on proposing a system but also on the optimal planning and sizing of the system. Palys et al. [22] compared the economics of hydrogen and ammonia storage using an optimal combined capacity planning and scheduling model. Islanded microgrids with renewable energy storage systems were evaluated in 15 cities with the goal of minimizing the leveled cost of energy. Liu et al. [23] investigated the optimal planning of a distributed hydrogen-based multi-energy system to minimize capital and operational costs. The optimal operation strategy was formulated as a mixed-integer linear programming (MILP) problem. The synergistic effect of hybrid energy and hot water storage on cost reduction was investigated. Assaf et al. [24] determined the optimal sizing of a solar-hydrogen combined heat and power system to maximize the system's overall reliability and minimize the levelized cost of electricity.

In the studies mentioned above, the backgrounds, assumptions, and conditions are quite different, i.e., the system configurations, operation strategies, supply and demand profiles, and nature of operations (on-grid or off-grid). The roles of the energy carriers were also different; they served either as a storage medium or as a product. Additionally, most studies focused on hydrogen-based systems. However, for an in-depth study of ammonia power generation systems, such as ammonia-fed fuel cells, the performance of ammonia as an energy carrier in a multi-generation system must be evaluated, which has not been extensively investigated. Thus, in this study, a hydrogen-based and an ammonia-based multi-generation systems with the same system configuration, operation strategy, and application background were developed. Rather than playing a single role, hydrogen and ammonia served as energy storage media, fuels, and products. Both hydrogen/ammonia storage systems and batteries were considered to enhance flexibility. The coupling of supply and demand was explicitly formulated based on an analytical model of each component. The performance of the system was evaluated based on weather and demand data collected hourly over a year. In each time interval, the scheduling of the system was described as an MLIP problem, in which the objective was to maximize revenue. Subsequently, the technical and economic performance was evaluated in terms of the average curtailment, cumulative cash position (CCP), and payback period (PBP). The main contributions of this study are summarized as follows.

- The feasibility of using hydrogen or ammonia as an energy carrier in a multi-generation system under the same conditions was comprehensively evaluated and compared.
- The effect of each component's capacity on profitability was analyzed through a sensitivity analysis.
- Additional scenarios involving different energy carriers, constant or time-of-use electricity prices, and on-grid or off-grid operations are discussed.

2. Materials and methods

Scenarios involving hydrogen- and ammonia-based systems, in which hydrogen and ammonia served as energy carriers in multi-generation systems, are first introduced. Appendix A presents the analytical and economic model of the system. The focus of this study was scenario analysis. In each scenario, an energy management system (EMS) provides optimal planning and is constructed as an MILP problem. Accordingly, the objective function and constraints of the problem are presented. Finally, the algorithm framework is described in detail.

2.1. Scenario descriptions

The hydrogen- and ammonia-based systems have a structure similar to that of an integrated renewable multi-generation system, consisting of a renewable farm, an energy storage system, and a hydrogen storage system, as shown in Fig. 1. The renewable farm consists of 20-MW solar PV systems and 20-MW wind turbines, providing green electricity to the demand side. Excess electricity is stored chemically and electrochemically if renewable energy is abundant. In contrast, fuel cells and batteries provide backup power in the event of an electricity shortage. The battery, water electrolysis, and fuel cell provide flexibility to the system operation and help the system overcome the problem of fluctuating supply and demand. The scheduling of these energy storage systems (electricity and hydrogen storage) is controlled using an EMS. The installed capacities of the water electrolysis, fuel cell, and battery were 15 MW, 15 MW, and 10 MWh, respectively. Direct (compressed hydrogen) and indirect (AS) hydrogen storage systems were considered because hydrogen storage for long-term energy storage is costly [25]. In this study, four scenarios, considering the effects of different energy carriers, constant or time-of-use electricity prices, and on-grid or off-grid operation were simulated and compared, as shown in Table 1. Scenarios S1–S3 involve hydrogen-based systems that use hydrogen as an energy carrier. Scenarios S2–S4 consider the time-of-use electricity price, providing more flexibility for the optimal planning of the system. Scenarios S1–S2 can be seen as islanded systems under off-grid operation, while scenarios S3–S4 allow the import of electricity from other areas.

2.2. Problem formulation

The EMS scheduled a multi-generation system to achieve flexible operation and maximum profits. The planning horizon was one year, with hourly time intervals. The system operation was studied using the analytical models described in **Appendix A**. Some assumptions were made before simulations:1) a quasi-stationary approach can be used because of the hourly time interval; 2) the system works under the ideal condition; 3) mass, pressure, and heat losses in pipelines can be neglected; 4) compressors and pumps work adiabatically; 5) the initial storage capacity is 50 % of the maximum capacity.

2.2.1. Objective function

The optimization problem is to determine the amount of electricity allocated to the dispatchable components of the system, including the battery, water electrolysis, fuel cell, and power grid. The objective function maximizes the benefit. This is expressed as follows.

$$\text{obj} = \max(REV_t - OPEX_t) \tag{1}$$

$$REV_t = \left(P^t_{\text{demand}} - P^t_{\text{g}}\right)C^t_{\text{ele}} + m^t_{\text{H}_2}C_{\text{H}_2} + m^t_{\text{NH}_3}C_{\text{NH}_3} + m^t_{\text{byproduct}}C_{\text{byproduct}} \tag{2}$$

$$OPEX_t = opex^t_{\text{rf}} + opex^t_{\text{es}} + opex^t_{\text{hs}} \tag{3}$$

REV_t and $OPEX_t$ denote the revenue and OPEX at time t, respectively; P^t_{demand} is the electricity demand; P^t_{g} is the imported electricity from the grid; C^t_{ele} is the time-of-use or constant electricity price; $m^t_{\text{H}_2}$ is the net rate of production of hydrogen, which is used only in scenarios using hydrogen-based systems; C_{H_2} is the constant hydrogen price; $m^t_{\text{NH}_3}$ is the net rate of production of ammonia, which is used only in scenarios using ammonia-based systems; $m^t_{\text{byproduct}}$ is the net rate of production of byproduct; $C_{\text{byproduct}}$ is the constant price of byproduct; $opex^t_{\text{rf}}$, $opex^t_{\text{es}}$, and $opex^t_{\text{hs}}$ are the OPEXs of the renewable farm, energy storage system, and hydrogen storage system, respectively.

2.2.2. Main constraints

Energy balance constraints are important. They were constructed as follows:

$$P^t_{\text{cur}} = P^t_{\text{rf}} \pm P^t_{\text{es}} - P^t_{\text{hs}} - P^t_{\text{as}} + P^t_{\text{g}} - P^t_{\text{demand}}, P^t_{\text{cur}} \geq 0, P^t_{\text{g}} \geq 0 \tag{4}$$

$$P^t_{\text{rf}} = P^t_{\text{PV}} + P^t_{\text{WT}} \tag{5}$$

$$P^t_{\text{es}} = \pm P^t_{\text{B}} - P^t_{\text{SOEL}} + P^t_{\text{SOFC}} \tag{6}$$

$$P^t_{\text{hs}} = P^t_{\text{C}} \tag{7}$$

$$P^t_{\text{as}} = P^t_{\text{AS}} + P^t_{\text{C}} \tag{8}$$

P^t_{cur} denote the renewable power curtailed at time t, P^t_{rf} is the output power of the renewable farm, P^t_{es} is the input or output power of the energy storage system, P^t_{hs} is the input power of the hydrogen storage system, P^t_{as} is the input power of the ammonia storage system, P^t_{PV} is the output power of PV systems, P^t_{WT} is the output power of the wind turbines, P^t_{B} is the input or output power of the battery, P^t_{SOEL} is the input power of solid oxide water electrolysis (SOEL), P^t_{SOFC} is the output power of the solid oxide fuel cell (SOFC), P^t_{C} is the output power of compression, and P^t_{AS} is the output power of the AS.

The input or output power of each component has limitations based on the analytical models, which can be approximated as follows:

The constraints of the renewable farm:

$$P^t_{\text{PV}} = \begin{cases} 0, P^t_{\text{cell}} \leq 0 \\ N_{\text{PV}}P^t_{\text{cell}}, 0 < P^t_{\text{cell}} \leq P_{\text{cell},rated} \end{cases}, \tag{9}$$

$$P^t_{\text{WT}} = \begin{cases} 0, v < 3 or v > 25 \\ N_{\text{WT}}P^t_{\text{turbine}}, 3 \leq v < 12 \\ N_{\text{WT}}P_{\text{turbine,rated}}, 12 \leq v \leq 25 \end{cases}, \tag{10}$$

where P^t_{cell} is the output power of the solar cell, N_{PV} is the installed number of solar cells $P_{\text{cell,rated}}$ is the rated power of the solar cell, v is the measured wind speed, N_{WT} is the number of wind turbines, P^t_{turbine} is the output power of the wind turbine, and $P_{\text{WT,rated}}$ is the rated power of the wind turbine. Notably, the solar cell is assumed to stop working under low temperature and low solar irradiance and the power from the PVs in the simulation result drops to less than zero, according to **Eqs.** (A1)–(A2).

Other constraints in the energy storage system are listed as follows:

$$0 \leq P^t_{\text{B}} \leq \text{P}_{\text{B,rated}} \tag{11}$$

$$SoC_{\min} \leq SoC_t \leq SoC_{\max} \tag{12}$$

$$0 \leq P^t_{\text{SOEL}} \leq x_{\text{SOEL}}P_{\text{SOEL,rated}} \tag{13}$$

$$0 \leq P^t_{\text{SOFC}} \leq x_{\text{SOFC}}P_{\text{SOFC,rated}} \tag{14}$$

$$x_{\text{SOEL}} + x_{\text{SOFC}} \leq 1, x_{\text{SOEL}}, x_{\text{SOFC}} \in \{0, 1\} \tag{15}$$

where $P_{\text{B,rated}}$ is the rated power of the battery; SoC_t is the state-of-charge (SoC) of the battery; $SoC_{\min}$ and $SoC_{\max}$ denote the minimum and maximum SoCs of the battery, respectively; x_{SOEL} and x_{SOFC} are the binary variables used to avoid producing and consuming hydrogen or ammonia at the same time, respectively; $P_{\text{SOEL,rated}}$ is the rated power of SOEL and $P_{\text{SOFC,rated}}$ is the rated power of the SOFC.

Another important constraint is the mass balance. The constraints of the hydrogen storage system are as follows:

$$m^t_{\text{H}_2,\text{sto}} = m^{t-1}_{\text{H}_2,\text{sto}} + m^t_{\text{H}_2,\text{SOEL}} - m^t_{\text{H}_2,\text{SOFC}} - m^t_{\text{H}_2,\text{loss}} - m^t_{\text{H}_2,\text{sold}} \tag{16}$$

$$M_{\text{H}_2,\min} \leq m^t_{\text{H}_2,\text{sto}} \leq M_{\text{H}_2,\max} \tag{17}$$

$$m^t_{\text{H}_2,\text{SOEL}} = \dot{m}_{\text{H}_2,\text{SOEL}}\frac{P^t_{\text{SOEL}} + P^t_{\text{C}}}{\dot{P}_{\text{SOEL}} + \dot{P}_{\text{C}}} \tag{18}$$

$$m^t_{\text{H}_2,\text{SOFC}} = \dot{m}_{\text{H}_2,\text{SOFC}}\frac{P^t_{\text{SOFC}}}{\dot{P}_{\text{SOFC}}} \tag{19}$$

where $m^t_{\text{H}_2,\text{sto}}$ is the amount of hydrogen stored at time t; $m^{t-1}_{\text{H}_2,\text{sto}}$ is the amount of hydrogen stored at time $t-1$; $m^t_{\text{H}_2,\text{SOEL}}$ is the rate of production of hydrogen from SOEL; $m^t_{\text{H}_2,\text{SOFC}}$ is the rate of consumption of hydrogen in SOFC; $m^t_{\text{H}_2,\text{loss}}$ is the amount of hydrogen lost during operation, which is set to 1 % of the production rate; $m^t_{\text{H}_2,\text{sold}}$ is the amount of hydrogen sold to the market; $M_{\text{H}_2,\min}$ and $M_{\text{H}_2,\max}$ are the maximum and minimum capacities of the hydrogen storage tank (STH), respectively. The production and consumption rates of hydrogen, $m^t_{\text{H}_2,\text{SOEL}}$ and $m^t_{\text{H}_2,\text{SOFC}}$ are assumed to be consistent with the simulation results of $\dot{m}_{\text{H}_2,\text{SOEL}}$ and $\dot{m}_{\text{H}_2,\text{SOFC}}$, respectively. $\dot{P}_{\text{SOEL}}$, $\dot{P}_{\text{SOFC}}$, and $\dot{P}_{\text{C}}$ are the input power of the SOEL, output power of the SOFC, and consumed power of the compression in the simulations, respectively.

Constraints on the ammonia storage system are similar to those of the hydrogen storage system.

$$m^t_{\text{NH}_3,\text{sto}} = m^{t-1}_{\text{NH}_3,\text{sto}} + m^t_{\text{NH}_3,\text{AS}} - m^t_{\text{NH}_3,\text{SOFC}} - m^t_{\text{NH}_3,\text{loss}} - m^t_{\text{NH}_3,\text{sold}} \tag{20}$$

$$M_{\text{NH}_3,\min} \leq m^t_{\text{NH}_3,\text{sto}} \leq M_{\text{NH}_3,\max} \tag{21}$$

$$m^t_{\text{NH}_3,\text{AS}} = \dot{m}_{\text{NH}_3,\text{AS}}\frac{P^t_{\text{SOEL}} + P^t_{\text{AS}} + P^t_{\text{C}}}{\dot{P}_{\text{SOEL}} + \dot{P}_{\text{AS}} + \dot{P}_{\text{C}}} \tag{22}$$

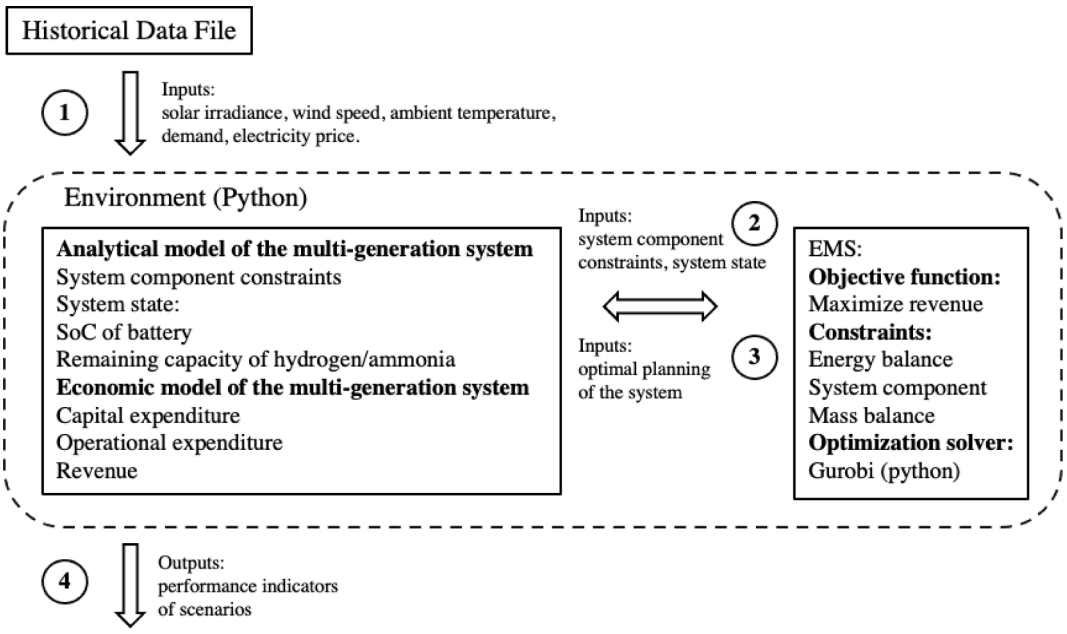

Fig. 2. Flowchart of the algorithm framework.

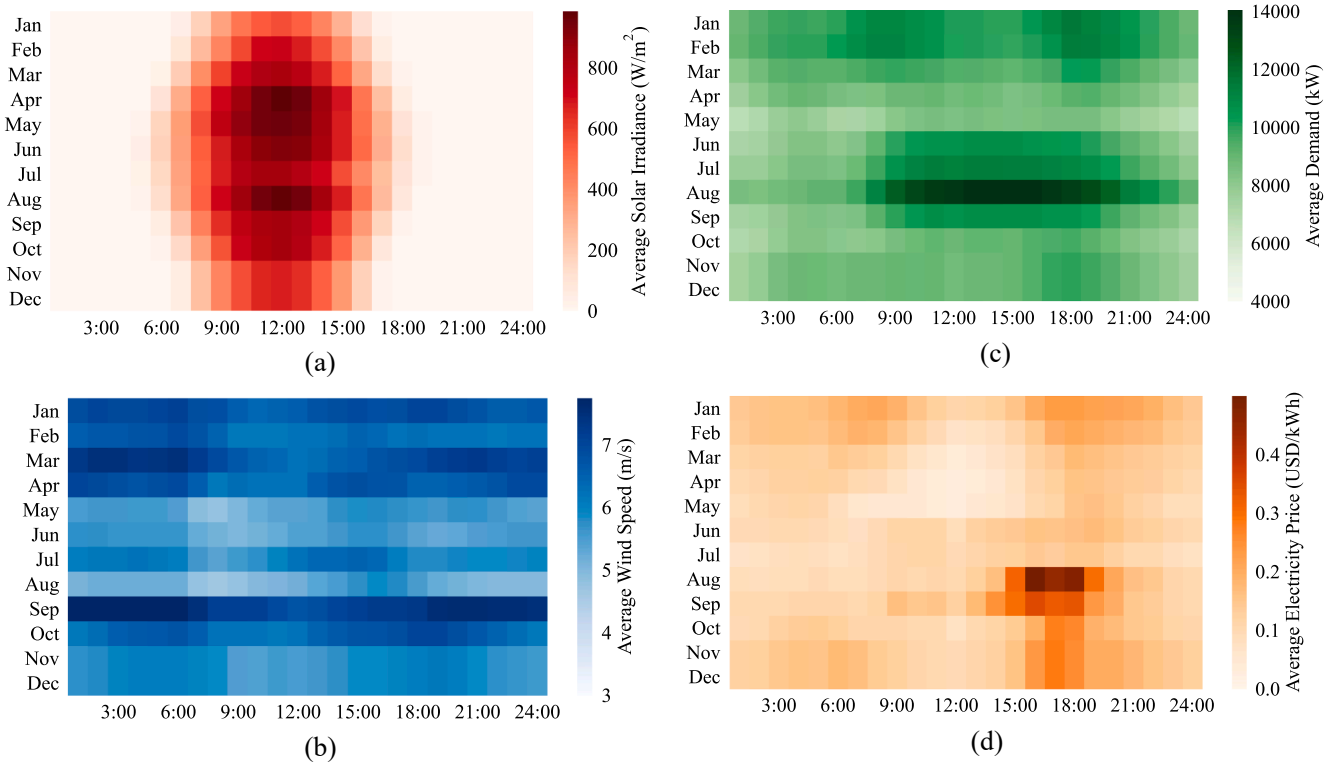

Fig. 3. Heat map of yearly distribution of solar irradiance (a) [27], wind speed (b) [28], demand (c), and electricity price (d) [29].

$$m^t_{NH_3,SOFC} = \dot{m}_{NH_3,SOFC}\frac{P^t_{SOFC}}{P_{SOFC}} \tag{23}$$

where $m^t_{NH_3,AS}$ are the rates of production of ammonia in the AS. The hydrogen produced by SOEL is directly used for ammonia production; therefore, there is no STH.

2.2.3. Performance indicator

Curtailment represents the technical performance of the system under each scenario, while CCP and PBP are used to evaluate the economic performance.

$$CCP = \sum_{j=1}^{n}\left(\frac{(REV - OPEX - d_j)\times(1-t)+d_j}{(1+i)^j}\right) - CAPEX \tag{24}$$

$$d_j = \frac{2}{n}\left(CAPEX - \sum_{k=1}^{j-1} d_k\right) \tag{25}$$

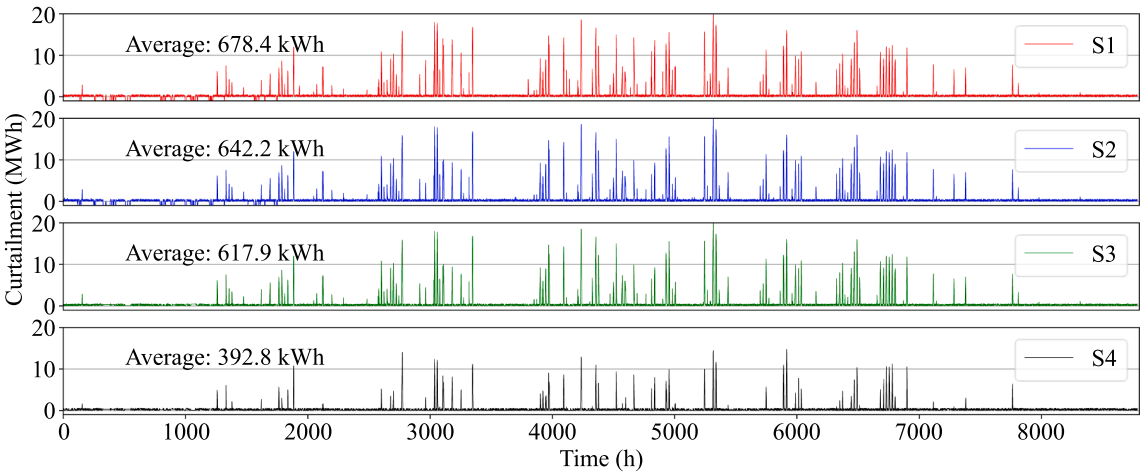

Fig. 4. Yearly distribution of curtailment in scenarios S1–S4.

where n is the system lifetime; *REV* is the annual revenue of the system; *OPEX* and *CAPEX* are the annual operational expenditure (OPEX) and capital expenditure (CAPEX) of the system, respectively, which were determined using the economic model given in **Appendix A**; d_j is the annual depreciation cost estimated via the double-declining balance depreciation method, as shown in **Eq.** (25), t is the tax rate, and i is the annual interest rate. PBP is the year when the CCP starts to turn positive.

2.3. Algorithm framework

An algorithm was developed to achieve the optimal planning of different scenarios. A flowchart is shown in Fig. 2, and detailed descriptions are provided below.

Step 1: Weather information and demand profiles, including solar irradiance, wind speed, ambient temperature, demand, and electricity price, were first collected. The historical data were used in this study. The analytical and economic models of the multi-generation system were initialized in a Python environment. Its details are given in **Appendix A**. The initial storage state of the energy and hydrogen storage systems was 50 % of the maximum capacity.

Step 2: In each time interval, according to the historical data, system state, and system constraints (**Eqs**. (1)–(25)), the EMS solved the objective function using the Gurobi optimizer [26]. The Gurobi optimizer is a powerful solver used for obtaining the optimal solution to a problem stated. Moreover, it can be directly used in the Python environment, which reduces the complexity of integrating different software packages.

Step 3: The result of the optimal planning was sent back to the system model to update the system state. Hourly simulation results were then recorded, including curtailment, system state, and revenue.

Step 4: Steps 2 and 3 were repeated during the 8784-h time span. The performance indicators were provided after a one-year simulation.

The performance of the system under the different scenarios can be evaluated easily using the proposed algorithm. It should be noted that this algorithm framework can be utilized in other scenario exploration without significant changes. First, historical data can be replaced by data from other areas or predictions from professional software. Second, the analytical and economic models can be modified using different system parameters, such as installed capacity and hydrogen price, because they are parameter-based models. Each component is independent of the others; hence, changing the configuration of the system is easy. For example, the hydrogen storage system can be changed to an ammonia storage system. Third, optimal planning can be formulated as a MILP problem that can be solved easily using the embedded Gurobi package.

Kyushu district in Japan was selected for the case study. Meteorological data, including net solar irradiance, wind speed at a height of 10 m, and ambient temperature, were obtained from the MERRA-2 database provided by the Global Modeling and Assimilation Office, Goddard Space Flight Center, and National Aeronautics and Space Administration [27,28]. Heat maps of the yearly distribution of solar irradiance and wind speed are shown in Fig. 3 **(a)** and Fig. 3 **(b)**, respectively. The figures show a strong uneven distribution of seasonal and daily solar irradiance. High solar irradiance mostly occurs around noon, between 10:00 a.m and 14:00p.m, whereas high wind speeds appear at night. The seasonal distribution also shows an opposite trend: solar energy is abundant in spring and summer. In contrast, wind energy is abundant in autumn, mostly in September. The demand profile and time-of-use electricity prices were collected from the Renewable Energy Institute of Japan [29]. The scale of the system was in megawatts; therefore, the demand profile was scaled down accordingly. Heat maps of the yearly distribution of demand and electricity price are shown in Fig. 3**(c)** and Fig. 3**(d)**, respectively. Kyushu district in Japan do not suffer from extreme weather conditions; hence, the electricity demands during the hot and cold months are satisfied by the electricity supplied. From June to September, there is a surge in electricity demand during working hours, especially in August. In addition, when heating demand increases in January and February, two relatively indistinctive peaks can be observed around 9:00 a.m. and 19:00p.m. The electricity price depends not only on the demand side but also on the supply side; therefore, a high electricity price corresponds to a high demand, but not vice versa.

3. Results and discussions

In this section, the performance of different scenarios is presented and analyzed. The performances under constant and time-of-use electricity prices, on– and off-grid operation, and hydrogen and ammonia as the energy carriers were compared. A sensitivity analysis of the system configurations was conducted to obtain further insights.

3.1. Technical performance

Fig. 4 depicts the yearly distribution of the curtailment under the four scenarios. Evidently, all four distributions have similar characteristics. This is because the configuration of the renewable energy farm remains the same under all scenarios. The peaks appear when the solar and wind outputs are significantly larger than the demand, such as in the first 1000 h when the output power of the renewable farm is relatively insufficient, and insufficient hydrogen is provided to the SOFC. During the off-grid operation of the system in scenarios S1 and S2, the installed capacity of the renewable energy farm and energy storage system cannot

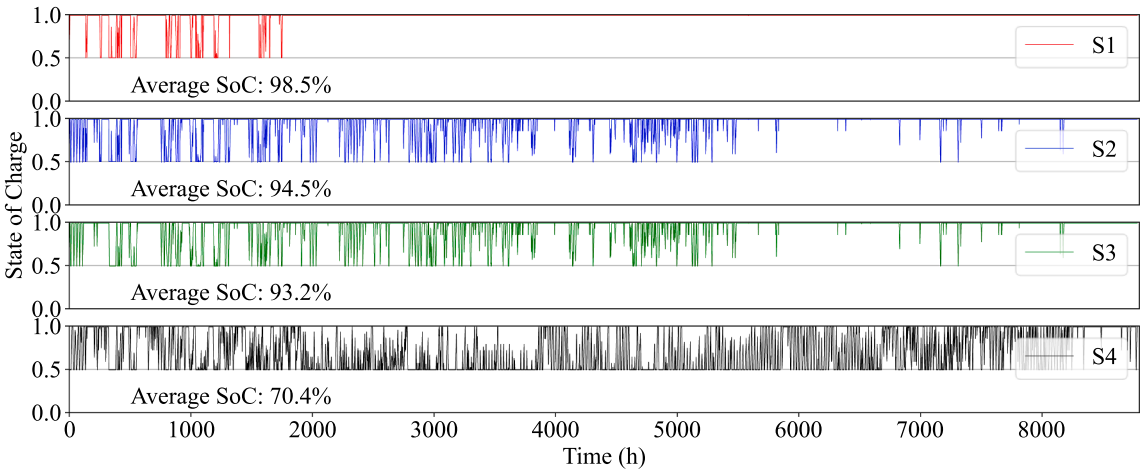

Fig. 5. Yearly distribution of battery storage in scenarios S1–S4.

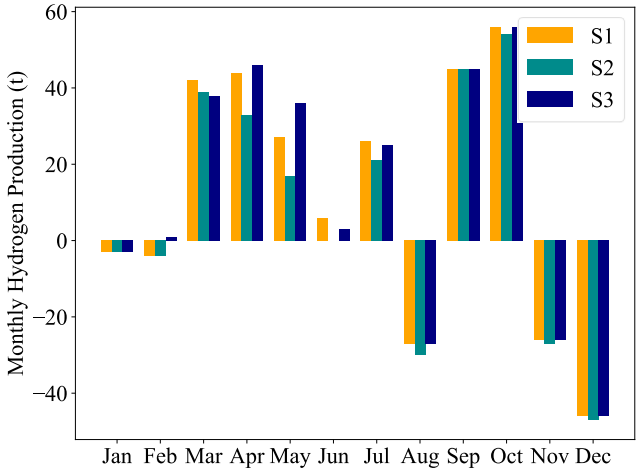

Fig. 6. Monthly distribution of net hydrogen production in scenarios S1–S3.

satisfy the demand in the beginning; therefore, the system stops working in those time intervals. To distinguish this from zero curtailment, a negative value is used to represent this situation, as shown in the figure. It should be noted that in the calculation, the output of the system in this situation was set to zero. The total working hours under scenarios S1 and S2 were 8540 and 8510 h, respectively, and those in scenarios S3 and S4 were 8784 h.

The average curtailment in S2 was lower than that in S1 because of the scheduling of the energy storage system. The priority over battery and hydrogen storage dynamically changed according to the time-of-use electricity price. In contrast, the priority remained unchanged in scenario S1 because both electricity and hydrogen prices were fixed. The battery charged during energy storage and discharged during the energy release. Therefore, the battery was less involved in the operation in S1 than in S2. This indicated that the energy that should have been stored in the battery was abandoned, thereby increasing the curtailment. The average curtailment further decreased in scenario S3 because the electricity imported from other areas eliminated the curtailment of electricity from the SOEL units when the electricity price was low. In scenario S4, the extra AS unit consumed more electricity; hence, the average curtailment declined by approximately 40 %.

The yearly distribution of the SoC is shown in Fig. 5. In scenario S1, because the utility cost of electricity for hydrogen production was higher than the revenue of the produced hydrogen and byproducts, the battery was used less in the system unless there was insufficient hydrogen for backup power. Thus, the battery operated only in the beginning. For the rest of the time, the accumulation of the produced hydrogen satisfied the need for SOFC units. Considering the time-of-use electricity price in scenarios S2–S4, battery storage was more involved in the operation. When the electricity price was high, excess electricity was sold to the battery to gain profit; hence, it full-charged rapidly under the full-load condition. If the excess electricity was insufficient, the SOFC units provided the required electricity. In contrast, when the price was low, the excess electricity was used to produce hydrogen. Similarly, the battery provided electricity to ensure the full-load operation of the SOEL units. After 6000 h, the operating times of battery storages in scenarios S2 and S3 decreased considerably because both demand and electricity prices were high in this period, as shown in Fig. 3. SOFC units were first used to fulfill the demand, and the battery remained full-charged.

The number of charge–discharge cycles of the battery under scenario S4 was the highest. At the same input power, the revenue from the ammonia-based system was higher than that from the hydrogen-based system because the rate of production of ammonia was considerably larger than that of hydrogen, and extra oxygen was produced from the air separation unit. Thus, they were less sensitive to high electricity prices. In most cases, excess electricity was used to produce and store ammonia, and this shortage of electricity was compensated by the battery.

The performance of hydrogen/ammonia storage was another important factor that affected the profitability of the system. The monthly distribution of the net hydrogen production in scenarios S1–S3 is shown in Fig. 6. The supply–demand balance and revenue have a significant influence on the production and consumption of hydrogen. Owing to the lack of renewable energy production in January and February, less excess electricity was used in SOEL units for hydrogen production, and SOFC units consumed hydrogen to provide backup power. Hence, in these two months, no hydrogen could be accumulated. However, in months with positive net hydrogen production, abundant renewable energy dominated the production. Demand and electricity prices were high in September, which indicated that excess electricity was stored in the battery first and mainly the SOFC units handled the shortage. However, renewable energy was still in surplus and a positive net hydrogen production was obtained. The increased negative net hydrogen production, that is, hydrogen consumption, in August, November, and December was caused by the higher output power of the SOF units. Because the storage system accumulated hydrogen in previous months, SOFC units had sufficient fuel for backup power generation. In contrast, in January and February, the stored electricity was insufficient; hence, the shortage of supply was not compensated by SOFC units alone.

The hydrogen consumption in scenario S2 was relatively higher than that in the other two scenarios. Compared with S1, the fluctuating

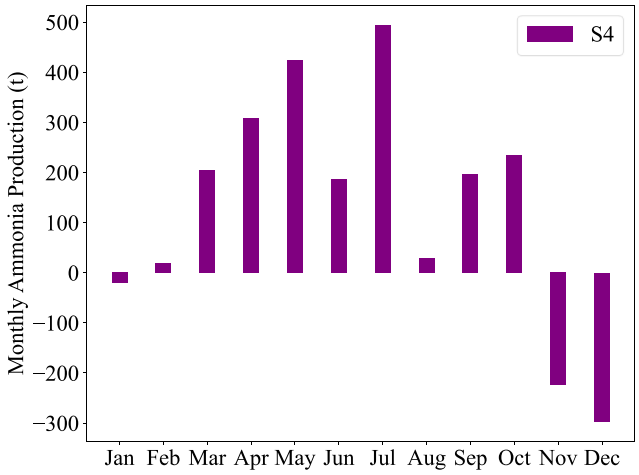

Fig. 7. Monthly distribution of net ammonia production in scenario S4.

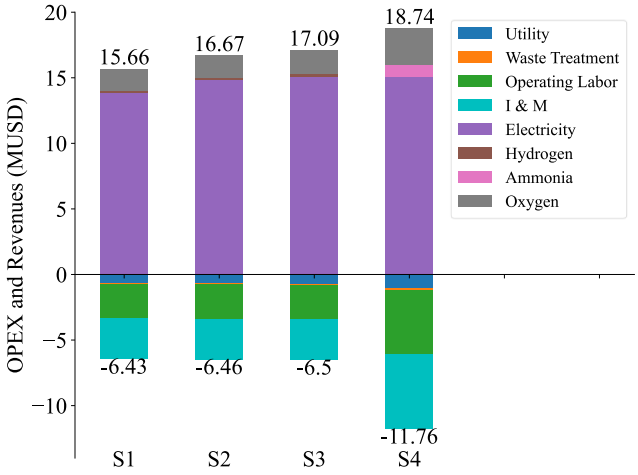

Fig. 9. Breakdown of OPEX and revenues in scenarios S1-4.

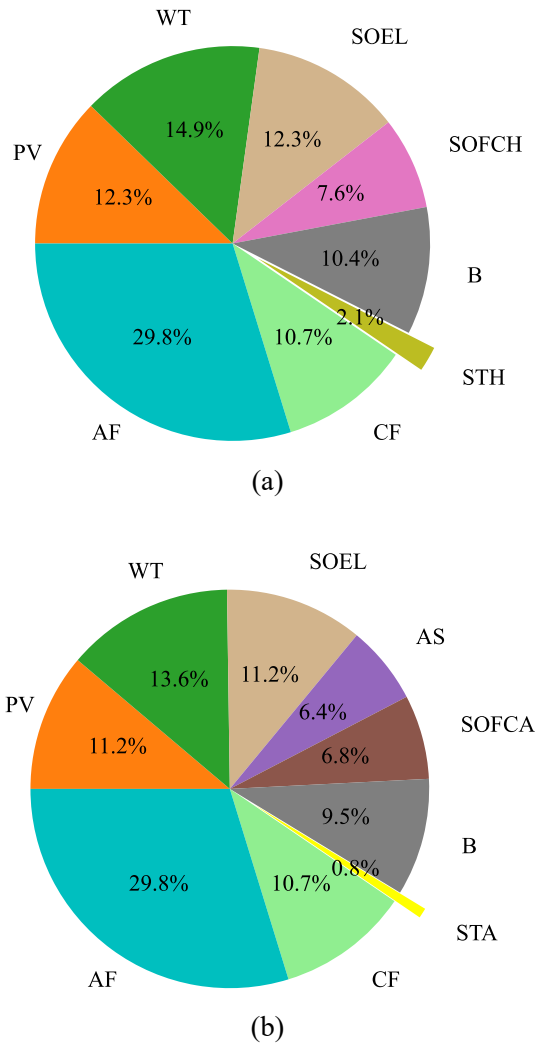

Fig. 8. Breakdown of CAPEXs of (a) hydrogen-based and (b) ammonia-based systems.

electricity price increased the frequency of conversion between hydrogen and electricity, during which energy and mass losses were incurred. Without any electricity imported from outside, SOEL units cannot maintain a sustained operation under full load conditions when the electricity price is low. It also impinges on the net hydrogen production. In contrast, in May, during which a lower electricity price and demand are observed, SOEL units can be guaranteed to produce more hydrogen in scenario S3 than in other scenarios because of the import of electricity.

Table 2
Configuration and profitability of scenarios S1–S4.

Name	PV (MW)	WT (MW)	SOEL (WM)	SOFC (MW)	Battery (MWh)	CCP (MUSD)	PBP (y)
S1	20	20	15	15	10	59.74	16
S2	20	20	15	15	10	77.09	15
S3	20	20	15	15	10	83.43	14
S4	20	20	15	15	10	12.78	22

The monthly distribution of the net ammonia production in scenario S4 is shown in Fig. 7. Essentially, it follows a trend similar to that observed under S3, except for a higher net production rate. Owing to the different profitability of hydrogen- and ammonia-based systems, the working hours of the ammonia production subsystem were longer than those of the hydrogen production subsystem. In addition, at the same input power, the amount of ammonia produced was larger than that of hydrogen.

3.2. Economic performance

The CAPEX and OPEX should be calculated before evaluating the economic performance of the system. Fig. 8. shows the breakdown of the CAPEXs of hydrogen- and ammonia-based systems. The renewable energy farm consumes approximately a quarter of the total CAPEX; the PV and WT systems cost 16.33 and 19.83 MUSD, respectively. Both systems also have the same SOEL and battery units, which cost 16.36 and 13.89 MUSD, respectively. The use of different energy carriers makes the capital costs of the SOFC and storage tanks slightly different. In the hydrogen-based system, the CAPEX of hydrogen-based SOFC (SOFCH) and STH are 10.06 and 2.73 MUSD, respectively, while in the ammonia-based system, the CAPEX of ammonia- based SOFC (SOFCA) and ammonia storage tank (STA) are 9.98 and 1.19 MUSD, respectively. This difference is attributed to the difference in the costs of the compressors and heat exchangers. Moreover, the AS subsystem in the ammonia-based system requires an extra 9.3 MUSD; hence, its total CAPEX (145.95 MUSD) is higher than that of the hydrogen-based system (133.05 MUSD).

The breakdown of OPEX and revenues in the four scenarios is shown in Fig. 9. It should be noted that the utility costs of hydrogen and ammonia are not considered during the OPEX calculation but was

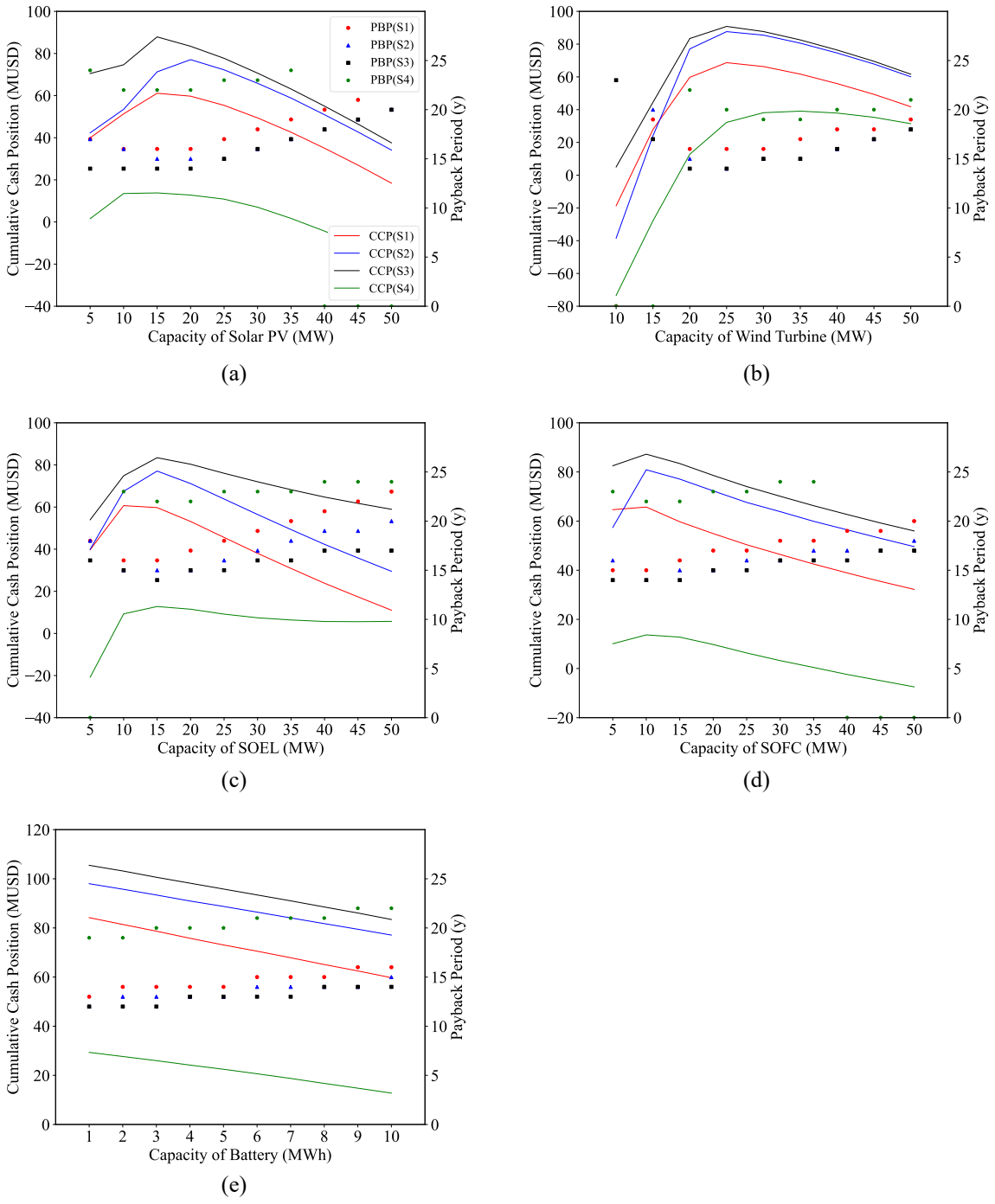

Fig. 10. Influence of installed capacity of PV units (a), wind turbines (b), SOEL units (c), SOFC units (d), and battery units (e) on the cumulative cash position (CCP) and payback period (PBP) of the multi-generation system, where dots denote payback period.

Table 3
Profitability of scenarios S3-4 and their variants.

Name	Energy carrier	PV (MW)	WT (MW)	SOEL (WM)	SOFC (MW)	Battery (MWh)	CCP (MUSD)	PBP (y)
S3	Hydrogen	20	20	15	15	10	83.43	14
S4	Ammonia	20	20	15	15	10	12.78	22
S5	Hydrogen	20	40	30	15	10	103.47	14
S6	Ammonia	20	40	30	15	10	97.82	15
S7	Hydrogen	20	20	15	15	–	107.93	12
S8	Ammonia	20	20	15	15	–	31.05	19

Table A1
CAPEX of the main components.

Description	CAPEX [USD]	Equipment cost attribute	Year	Ref.
Solar PV	1340	1 kW	2019	[42]
Wind Turbine	1514	1 kW	2019	[43]
Solid Oxide Stack	337	1 kW	2018	[44]
Battery	236	1 kWh	2017	[45]
Membrane	1000	1 ft^2	2009	[46]

Table A2
Assumptions for OPEX estimation.

Description	Value	Unit	Ref.
System lifetime	25	y	–
Stack lifetime	10	y	–
Battery lifetime	5	y	–
Membrane lifetime	5	y	–
Hydrogen price	1500	USD·t^{-1}	[12]
Ammonia price	514	USD·t^{-1}	[48]
Oxygen price	177	USD·t^{-1}	[8]
Electricity price	160	USD·MWh^{-1}	[49]
Process water price	2.45	USD·t^{-1}	[50]
Cooling water price	0.067	USD·t^{-1}	[50]
Heating price	12.33	USD·GJ^{-1}	[50]
Cooling price	4.43	USD·GJ^{-1}	[50]
Refrigeration price	7.89	USD·GJ^{-1}	[50]
Catalyst price (ASR)	20	USD·kg^{-1}	[47]

considered during revenue calculation. Operating labor, insurance, and maintenance (I & M) costs account for the majority of the OEPX, which is correlated with CAPEX; hence, the total OPEX of the ammonia-based system is higher than that of the hydrogen-based system. The utility and waste treatment costs play a minor role depending on the working hours and capacity of each subsystem. The higher rate of production of ammonia necessitates more investments on utility and waste treatment. Selling electricity earns approximately 13–15 MUSD per year. Adopting the time-of-use electricity price in S2 increases the revenue by 1 MUSD compared to that in S1, while allowing electricity import in S3 and S4 increases another 0.2 MUSD. However, owing to the lower accumulation of hydrogen and ammonia, the only gains in S1–S3 and S4 were 0.2 MUSD and 0.9 MUSD, respectively. In addition, the revenue from oxygen production was approximately 1.7 MUSD in S1–S3 and 2.8 MUSD in S4.

After obtaining the CAPEX and OPEX, the profitability can be evaluated using **Eq.** (24). The configuration and profitability of scenarios S1–S4 are shown in Table 2. In the hydrogen-based scenario S1, where the electricity price is constant, exhibited a CCP of 59.74 MUSD and a PBP of 16 units. Adopting the time-of-use electricity pricing considerably improves the profitability in scenario S2, as it improves the flexibility of the scheduling of the energy storage system. Moreover, importing electricity from other areas in scenario S3 resulted in further improvement in profitability. This is because, in scenario S3, when the time-of-use electricity price is low, SOEL units operate at a rated power, which increases the hydrogen production rate and is beneficial to revenue. The CCP and PBP in scenario S3 were acceptable to stakeholders. S4 exhibited a similar trend; therefore, only the optimal scenario considering both the time-of-use electricity price and electricity imports has been shown. Its profitability was the worst because the annual revenue is not high enough to cover the CAPEX and OPEX.

3.3. Sensitivity analysis

In previous simulations, the capacity of each subsystem was determined based on the scale of electricity demand. CAPEX, OPEX, and annual revenue are highly related to capacity and system configuration. Therefore, to increase profitability, a trade-off must be applied between decreasing CAPEX and OPEX and increasing annual revenue. Additional simulations were conducted to determine the effects of the capacity and configuration on the system profitability. In these simulations, the variations in the capacities of solar PVs, wind turbines, SOEL units, SOFC units, and batteries were considered, as shown in Fig. 10. The base configurations are listed in Table 2.

Generally, the basic trend is similar to that under the base configuration in that S3 is optimal and S4 is the worst. Except in Fig. 10 **(e)** (battery units), CCP first increases and then decreases with increasing installed capacity. As shown in Fig. 10 **(a)-(b)**, as the capacity of wind turbines decreases (depicted in Fig. 9 (b)), the CCP sharply reduces, and even reaches a negative value. The CCP reduces as the capacity of solar PVs increases (depicted in Fig. 9 (a)); however, the rate of reduction is not as high as that of the reduction with the decreasing capacity of wind trubines. As the capacity of wind turbines increases, the negative effect of capacity on the CCP becomes weaker than that of solar PVs. In terms of profitability, a high proportion of wind turbines is preferable. Slightly decreasing the capacity of solar PVs and increasing the capacity of wind turbines increase the benefit compared to that of the base configuration. In addition, with the increase in the installed capacity of renewable energy, the CCPs in scenarios S2 and S3 converge and their PBPs overlap. In scenario S3, sufficient renewable energy decreases the amount of electricity imported from other areas; hence, S2 and S3 become the same. In this case, the capacity of SOEL units restricts the revenue from hydrogen production.

The behavior exhibited in Fig. 10 **(c)** can be explained as follows. Although more SOEL units increase the production rates of hydrogen and ammonia, they are still limited by the lack of excess electricity, and the increase in the corresponding revenue cannot compensate for the increment of CAPEX and OPEX. In scenarios S3 and S4, electricity is purchased from other areas when the time-of-use electricity price is low; hence, the SOEL units operate under the full load condition as much as possible. However, S4 exhibits a lesser negative effect of increasing capacity than others because the ammonia-based system is less sensitive to the electricity price, as mentioned before. It is advisable to increase the capacity of the SOEL units only. This increase was accompanied by an increase in the installed capacity of renewable energy.

The CCP decreases as the capacity of SOFC units increases, as shown in Fig. 10 **(d)**. During the off-grid operation of the system (S1–S2), if the capacity of the SOFC units is decreased, the lack of electricity may not be compensated by the remaining SOFC and battery units, which is not reflected in the CCP. In contrast, during the on-grid operation of the system, the lack of electricity is compensated by purchasing electricity, which increases the OPEX because the electricity price is probably high at this time. This causes a sharp decline in the CCP in scenario S3 with the decrease in the number of SOFC units. In Fig. 10 **(e)**, the correlation between CCP and the number of battery units is linear because the SOFC units can satisfy the deficiency alone. Therefore, off-grid operation must be equipped with backup power if sustained operation has to be maintained. In addition, having backup power in the on-grid operation of the system enables it to operate more flexibly according to the varying prices.

3.4. General discussion

For the off-grid operation of the system (S1-S2), sustaining a continuous operation for a long time is difficult because of the seasonal uneven distribution feature of renewable energy, unless renewable farms and energy storage systems have a high capacity to cover the gap between the periods of sufficient and insufficient renewable energy. A higher capacity indicates higher CAPEX and OPEX. This also results in low average utilization rates of the energy storage systems. Both have negative effects on profitability. In contrast, the on-grid operation of the system (S3-S4) is more flexible and presents better performance in terms of technical and economic aspects. This method has the potential for further improvement. Based on the optimal hydrogen- and ammonia-based scenarios S3 and S4, two changes were made for discussion

according to the sensitivity analysis. In scenarios S5 and S6, the system doubled the capacity of the wind turbine and SOEL, whereas in scenarios S7 and S8, the system did not use any battery. A comparison is presented in Table 3.

The revenue from selling fuel (hydrogen or ammonia) is increased if the power-to-fuel capacity (renewable farm and SOEL units) is increased significantly. The increase in capacity increases the rate of production of hydrogen, which increases the profit of the system in scenario S5 by 20 MUSD. Nevertheless, the same change causes the profit in scenario S6 to increase nearly sevenfold and the PBP decreases to 16. This is because ammonia-to-power conversion is not as profitable as hydrogen-to-power conversion most of the time owing to the current price of ammonia. Hence, as the capacity of renewable energy increases, the use of ammonia fuel cells decreases; meanwhile, the production rate of ammonia increases. They both increase the net production rate of ammonia, which further improves the profitability of the ammonia-based system. Decreasing the CAPEX of the system is another method for improving profitability. As shown in Fig. 10, decreasing the capacity of the battery has only a positive effect on profitability. In scenarios S7 and S8, the CCP and PBP exhibit a remarkable improvement. This is because the operation of the battery has no direct effect on the revenue. It provides more flexibility with respect to the time-of-use electricity price, which indeed earns more benefits. However, the gain cannot cover the CAPEX. Under these circumstances, the role of the battery can be determined by the SOFC and grid. The reason for maintaining the battery in the system is its fast response characteristic.

4. Conclusions

In this study, a techno-economic evaluation of hydrogen and ammonia as energy carriers in multi-generation systems was conducted and compared. The operation of the system was formulated as a MILP problem, which was solved using a commercial solver. Through scenario analysis, the effects of different energy carriers, constant or time-of-use electricity prices, and on– or off-grid operation on the system performance were determined. Additionally, the sensitivity analysis provides insights into system configurations, and the suggestions are provided accordingly. The conclusions are summarized as follows:

In general, with the same proposed configuration, a hydrogen-based system is superior to an ammonia-based system in terms of profitability. In the optimal hydrogen-based scenarios, the CCP was 83.43 MUSD and the PBP was 14 years. CCP and PBP were 12.78 MUSD and 22 years, respectively, in the optimal ammonia-based scenario. Although the curtailment was reduced and the production of selling products was higher in the ammonia-based system, they could not cover the increment in CAPEX and OPEX.

To improve profitability, it is better to increase the proportion of the wind output and reduce the capacity of the backup power system (fuel cells and batteries) as much as possible. If the power-to-fuel capacity (renewable farm and SOEL units) is increased significantly, the profitability of the ammonia-based system approaches that of the hydrogen-based system. However, the system is limited by the green hydrogen or ammonia production, rather than power generation. In addition, both the battery and fuel-to-power restrict the profitability of the system, which requires further improvement in terms of operation and manufacture.

The off-grid operation of the system can hardly be sustained unless there is a high capacity for renewable farms and energy storage systems to overcome the seasonal uneven distribution of renewable energy. However, this results in high curtailment, low efficiency, and poor profitability. In contrast, the on-grid operation of the system is more flexible in terms of the fluctuant supply, demand, and prices.

CRediT authorship contribution statement

Du Wen: Conceptualization, Methodology, Software, Writing – original draft. **Shicheng Liu:** Data curation, Investigation. **Zhiyuan Ning:** Data curation, Investigation. **Muhammad Aziz:** Supervision, Validation, Resources, Writing – review & editing.

Declaration of Competing Interest

The authors declare that they have no known competing financial interests or personal relationships that could have appeared to influence the work reported in this paper.

Data availability

No data was used for the research described in the article.

Acknowledgments

This work was supported by JST SPRING (grant number JPMJSP2108).

Appendix A

A.1. Analytical model

The analytical model is formulated and approximated mathematically to express the operation of a multi-generation system based on a previous study [34].

A.1.1. Renewable farm

Renewable farms include solar PVs and wind turbines. The analytical model of solar PV was constructed based on reference [30], which considers the influence of solar irradiance and ambient temperature.

$$P_{PV} = N_{PV}\eta_{ref}A_{PV}I\left[1+\delta\left(t_c - t_{ref}\right)\right] \tag{A1}$$

$$t_c = \frac{26.6t_a + I\left[\tau\alpha - \eta_{ref}\left(1-\delta t_{ref}\right)\right]}{26.6 + \delta\eta_{ref}I} \tag{A2}$$

where P_{PV} is the output power of the solar PV, [kW]; N_{PV} is the number of solar cells, [–]; η_{ref} is the conversion efficiency of the solar cells at the reference temperature, 0.187 [–]; A_{PV} is the area of a single solar cell, [m^2]; I is the solar irradiance, [$kW{\cdot}m^{-2}$]; δ is the temperature coefficient, 0.38 [$\%{\cdot}{}^{\circ}C^{-1}$]; t_c is the cell temperature without considering wind speed, [°C]; t_{ref} is the reference temperature, 25 [°C]; t_a is the ambient temperature, [°C]; and $\tau\alpha$ is the optical parameter of the solar cell, 0.81 [–]. Spectral and angular impacts [31] are omitted here. For the wind turbine, the typical piecewise power curve is used [32], as follows:

$$P_{WT} = 0.5 N_{WT} \rho A_{WT} C_p v^3 \tag{A3}$$

$$v = v_g \left(\frac{h}{h_g}\right)^{\beta} \tag{A4}$$

where P_{WT} is the output power of wind turbines, [kW]; N_{WT} is the number of wind turbines, [–]; ρ is the air density, 1.255 [kg·m^{-3}]; A_{WT} is the swept area of a single wind turbine, [m^3]; C_p is the power coefficient, 0.49 [–]; v is the wind speed, [m·s^{-1}]; v_g is the measured wind speed near the ground, [m·s^{-1}]; h is the height of rotor, [m]; h_g is the height of measurement, [m]; and β is the wind shear exponent, 0.16 [–] [33]. The cut-in, rated, and cut-off speeds were 3 m·s^{-1}, 12 m·s^{-1}, and 25 m·s^{-1}, respectively [34]. The wake effect was neglected in this study.

A.1.2. Energy storage system

The state of charge (SoC) denotes the remaining power in the battery, which is defined as

$$E_t = E_{t-1} + \eta_c P_c = E_{t-1} - \frac{P_d}{\eta_d} \tag{A5}$$

$$SoC_t = SoC_{t-1} \pm \frac{E_t}{E_B} \tag{A6}$$

where E_t is the stored energy at time t, [kWh]; η_c is the charging efficiency, 0.8 [–]; P_c is the charging power, [kW]; η_d is the discharging efficiency, 0.8 [–]; P_d is the discharging power, [kW]; SoC_t is the state of charge at time t, [–] and E_B is the maximum storage capacity of the battery [A·h]. It should be noted that battery voltage is a function of SoC and current [35]. Because the time interval was relatively high (hour), the power and efficiency of the battery were assumed to be constant in each time interval. The degradation, which depends on the number of cycles [36], is not considered here but in the calculation of CAPEX.

Solid oxide water electrolysis (SOEL) technology was chosen because of its higher power density and efficiency [37] than those of other technologies. However, a solid oxide cell can not only convert steam into hydrogen and oxygen but also realize a reversible process [38]. Therefore, solid oxide fuel cells (SOFC) and SOEL were chosen for hydrogen production and backup power generation, respectively. An extra ammonia synthesis (AS) subsystem was added to the ammonia-based system. The SOEL, SOFC, and AS were simulated using ASPEN Plus V11 (Aspen Technology Inc.) [39]. The simulation results are presented in **Appendix B**. It should be noted that the remaining fuel in the resulting gas is usually burnt for power generation; however, in this study, because the scale of the SOFC was not sufficiently large, membrane separation technology was used to collect the remaining fuel. The hydrogen and ammonia produced were compressed into the storage tank for later use. The electricity consumed owing to adiabatic compression can be expressed as [40]

$$P_C = \frac{R T_{in}}{2(\gamma - 1)\eta_c} \left(\left(\frac{P_{out}}{P_{in}}\right)^{\frac{\gamma-1}{\gamma}} - 1 \right) m_g \tag{A7}$$

where P_C is the input power of the compressor [kW], T_{in} is the inlet temperature of the gas [K], γ is the isotropic exponent (1.4 [–], η_c is the compression efficiency (0.8 [–], and m_g is the mass flow rate of the gas, [kg·h^{-1}].

A.2. Economic model

Profitability of the proposed scenarios is an important factor for stakeholders; hence, CAPEX and OPEX were considered.

A.2.1. CAPEX

The CAPEX of the system was estimated based on the method described in [19]. The main components with available CAPEX data (solar PV, wind turbine, solid oxide stack, battery, and membrane) can be directly borrowed from references, as shown in Table A1, and corrected with the equipment cost attribute and inflation via **Eq.** (A8). Expenditure on components such as the compressor, pump, heater, cooler, heat exchanger, reactor, and process vessel are evaluated using the bare module cost. It is mathematically evaluated using an empirical equation, in which the capacity, material, operating temperature, and operating pressure play a major role. Considering auxiliary facilities, contingency, and fee costs, a specific value is multiplied by the bare model cost. The summation of these is the grassroots cost, which was considered as the CAPEX in this study, as presented in **Eq.** (A9). Finally, all costs were corrected using the chemical engineering plant cost index (CEPCI).

$$CAPEX_i = \left(\frac{A_i}{A_b}\right)^n CAPEX_b \left(\frac{I_t}{I_0}\right) \tag{A8}$$

$$CAPEX = C_{BM} + C_{CF} + C_{AF} + C_{land} \tag{A9}$$

where $CAPEX_i$ is the CAPEX of component i; A_i is the equipment cost attribute of component i which can be the capacity or production rate; n is cost exponent taken from [41]; $CAPEX_b$ is the CAPEX of a component on the baseline condition in the reference; when considering the inflation, I_t and I_0 are the cost indices (CEPCI) at the desired time and base time, respectively; C_{BM} is the bare module cost; C_{CF} is the contingency and fee costs which are set to 0.18 C_{BM}; C_{AF} is the auxiliary facilities costs which are set to 0.5 C_{BM}; and C_{land} is the cost of land use, which is 5 % of CAPEX.

A.2.2. OPEX

The OPEX of the system can be estimated based on [47]:

$$OPEX = C_{RM} + C_{UT} + C_{WT} + C_{OL} + C_{IM} \tag{A10}$$

where C_{RM} is the cost of the raw material, C_{UT} is the utility cost, including water, heating, and cooling. Under on-grid operation, imported electricity was considered. C_{WT} is the cost of waste treatment. After hydrogen/ammonia separation, the remaining gas should be handled. C_{OL} is the cost of operating labor and is affected by the number of process steps, and C_{IM} is the cost of insurance and maintenance, which is set to 2.3 % of CAPEX. The assumptions for OPEX are listed in Table A2.[27].

References

[1] Tashie-Lewis BC, Nnabuife SG. Hydrogen Production, Distribution, Storage and Power Conversion in a Hydrogen Economy - A Technology Review. Chem Eng J Adv 2021;8:100172.
[2] Falcone PM, Hiete M, Sapio A. Hydrogen economy and sustainable development goals: Review and policy insights. Curr Opin Green Sustainable Chem 2021;31:100506.
[3] Younas M, Shafique S, Hafeez A, Javed F, Rehman F. An Overview of Hydrogen Production: Current Status, Potential, and Challenges. Fuel 2022;316:123317.
[4] Hassan IA, Ramadan HS, Saleh MA, Hissel D. Hydrogen storage technologies for stationary and mobile applications: Review, analysis and perspectives. Renew Sustain Energy Rev 2021;149:111311.
[5] Fan L, Tu Z, Chan SH. Recent development of hydrogen and fuel cell technologies: A review. Energy Rep 2021;7:8421–46.
[6] Tarhan C, Çil MA. A study on hydrogen, the clean energy of the future: Hydrogen storage methods. J Storage Mater 2021;40:102676.
[7] Fasihi M, Weiss R, Savolainen J, Breyer C. Global potential of green ammonia based on hybrid PV-wind power plants. Appl Energy 2021;294:116170.
[8] Zhang H, Wang L, Van Herle J, Maréchal F, Desideri U. Techno-economic comparison of green ammonia production processes. Appl Energy 2020;259:114135.
[9] Afif A, Radenahmad N, Cheok Q, Shams S, Kim JH, Azad AK. Ammonia-fed fuel cells: a comprehensive review. Renew Sustain Energy Rev 2016;60:822–35.
[10] Cardoso JS, Silva V, Rocha RC, Hall MJ, Costa M, Eusébio D. Ammonia as an energy vector: Current and future prospects for low-carbon fuel applications in internal combustion engines. J Clean Prod 2021;296:126562.
[11] Cesaro Z, Ives M, Nayak-Luke R, Mason M, Bañares-Alcántara R. Ammonia to power: Forecasting the levelized cost of electricity from green ammonia in large-scale power plants. Appl Energy 2021;282:116009.
[12] Hydrogen Council. Hydrogen Insights: A perspective on hydrogen investment, market development and cost competitiveness. Available at: https://hydrogencouncil.com/en/hydrogen-insights-2021/.
[13] Luqman M, Bicer Y, Al-Ansari T. Thermodynamic analysis of an oxy-hydrogen combustor supported solar and wind energy-based sustainable polygeneration system for remote locations. Int J Hydrogen Energy 2020;45:3470–83.
[14] Siddiqui O, Dincer I. Design and analysis of a novel solar-wind based integrated energy system utilizing ammonia for energy storage. Energ Conver Manage 2019;195:866–84.
[15] Karapekmez A, Dincer I. Thermodynamic analysis of a novel solar and geothermal based combined energy system for hydrogen production. Int J Hydrogen Energy 2020;45:5608–28.
[16] Ozturk M, Dincer I. Thermodynamic analysis of a solar-based multi-generation system with hydrogen production. Appl Therm Eng 2013;51:1235–44.
[17] Shahid UB, Bicer Y, Ahzi S, Abdala A. Thermodynamic assessment of an integrated renewable energy multi-generation system including ammonia as hydrogen carrier and phase change material energy storage. Energ Conver Manage 2019;198:111809.
[18] Alirahmi SM, Razmi AR, Arabkoohsar A. Comprehensive assessment and multi-objective optimization of a green concept based on a combination of hydrogen and compressed air energy storage (CAES) systems. Renew Sustain Energy Rev 2021;142:110850.
[19] Singh A, Baredar P, Gupta B. Techno-economic feasibility analysis of hydrogen fuel cell and solar photovoltaic hybrid renewable energy system for academic research building. Energ Conver Manage 2017;145:398–414.
[20] Şevik S. Techno-economic evaluation of a grid-connected PV-trigeneration-hydrogen production hybrid system on a university campus. Int J Hydrogen Energy 2022;47:23935–56.
[21] Arnaiz del Pozo C, Cloete S. Techno-economic assessment of blue and green ammonia as energy carriers in a low-carbon future. Energ Conver Manage 2022;255:115312.
[22] Palys MJ, Daoutidis P. Using hydrogen and ammonia for renewable energy storage: A geographically comprehensive techno-economic study. Comput Chem Eng 2020;136:106785.
[23] Liu J, Xu Z, Wu J, Liu K, Guan X. Optimal planning of distributed hydrogen-based multi-energy systems. Appl Energy 2021;281:116107.
[24] Assaf J, Shabani B. Multi-objective sizing optimisation of a solar-thermal system integrated with a solar-hydrogen combined heat and power system, using genetic algorithm. Energ Conver Manage 2018;164:518–32.
[25] Rouwenhorst KHR, Van der Ham AGJ, Mul G, Kersten SRA. Islanded ammonia power systems: Technology review & conceptual process design. Renew Sustain Energy Rev 2019;114:109339.
[26] L. Gurobi Optimization, Gurobi Optimizer Reference Manual. Available at: https://www.gurobi.com, (2022).
[27] Global Modeling and Assimilation Office (GMAO) (2015), MERRA-2 tavg1_2d_rad_Nx: 2d,1-Hourly,Time-Averaged,Single-Level,Assimilation,Radiation Diagnostics V5.12.4, Greenbelt, MD, USA, Goddard Earth Sciences Data and Information Services Center (GES DISC), Accessed: [Data Access Date], 10.5067/Q9QMY5PBNV1T.
[28] Global Modeling and Assimilation Office (GMAO) (2015), MERRA-2 inst1_2d_lfo_Nx: 2d,1-Hourly,Instantaneous,Single-Level,Assimilation,Land Surface Forcings V5.12.4, Greenbelt, MD, USA, Goddard Earth Sciences Data and Information Services Center (GES DISC), Accessed: [Data Access Date], 10.5067/RCMZA6TL70BG.
[29] Power Supply & Demand Chart: All Japan, Renewable Energy Institute of Japan. Available at: https://www.renewable-ei.org/en/statistics/electricity/#demand.
[30] Shi Y, Sun Y, Liu J, Du X. Model and stability analysis of grid-connected PV system considering the variation of solar irradiance and cell temperature. Int J Electr Power Energy Syst 2021;132:107155.
[31] Lindsay N, Libois Q, Badosa J, Migan-Dubois A, Bourdin V. Errors in PV power modelling due to the lack of spectral and angular details of solar irradiance inputs. Sol Energy 2020;197:266–78.
[32] Lydia M, Kumar SS, Selvakumar AI, Prem Kumar GE. A comprehensive review on wind turbine power curve modeling techniques. Renew Sustain Energy Rev 2014;30:452–60.
[33] Pishgar-Komleh SH, Keyhani A, Sefeedpari P. Wind speed and power density analysis based on Weibull and Rayleigh distributions (a case study: Firouzkooh county of Iran). Renew Sustain Energy Rev 2015;42:313–22.
[34] Wen D, Aziz M. Flexible operation strategy of an integrated renewable multi-generation system for electricity, hydrogen, ammonia, and heating. Energ Conver Manage 2022;253:115166.
[35] Aaslid P, Geth F, Korpås M, Belsnes MM, Fosso OB. Non-linear charge-based battery storage optimization model with bi-variate cubic spline constraints. J Storage Mater 2020;32:101979.
[36] García-Miguel PLC, Asensio AP, Merino JL, Plaza MG. Analysis of cost of use modelling impact on a battery energy storage system providing arbitrage service. J Storage Mater 2022;50:104203.
[37] Cinti G, Frattini D, Jannelli E, Desideri U, Bidini G. Coupling Solid Oxide Electrolyser (SOE) and ammonia production plant. Appl Energy 2017;192:466–76.
[38] Kupecki J, Motylinski K, Jagielski S, Wierzbicki M, Brouwer J, Naumovich Y, et al. Energy analysis of a 10 kW-class power-to-gas system based on a solid oxide electrolyzer (SOE). Energ Conver Manage 2019;199:111934.
[39] Aspen Tech, Aspen Plus Simulation Software, 2021. Available at: http://www.aspentech.com/products/aspen-plus/.
[40] Klyapovskiy S, Zheng Y, You S, Bindner HW. Optimal operation of the hydrogen-based energy management system with P2X demand response and ammonia plant. Appl Energy 2021;304:117559.
[41] Robert James, Alexander Zoelle, Norma Kuehn. Quality Guidelines For Energy System Studies - Capital Cost Scaling Methodology: Revision 4 Report, U.S. Department of Energy National Energy Technology Laboratory; 2019.
[42] Annual Technology Baseline. NREL, 2021. Available at: https://atb.nrel.gov/electricity/2021/utility-scale_pv.
[43] Annual Technology Baseline. NREL, 2021. Available at: https://atb.nrel.gov/electricity/2021/land-based_wind.
[44] Anghilante R, Colomar D, Brisse A, Marrony M. Bottom-up cost evaluation of SOEC systems in the range of 10–100 MW. Int J Hydrogen Energy 2018;43:20309–22.
[45] Ralon P, Taylor M, Ilas A, Diaz-Bone H, Kairies K. Electricity storage and renewables: Costs and markets to 2030. Abu Dhabi, UAE: International Renewable Energy Agency; 2017.
[46] Cloete S, Khan MN, Nazir SM, Amini S. Cost-effective clean ammonia production using membrane-assisted autothermal reforming. Chem Eng J 2021;404:126550.
[47] DOE/NETL. Cost and Performance Baseline for Fossil Energy Plants Volume 2: Coal to Synthetic Natural Gas and Ammonia. vol. 2; 2011. https://doi.org/DOE/NETL-2010/1402.
[48] Andersson J, Lundgren J. Techno-economic analysis of ammonia production via integrated biomass gasification. Appl Energy 2014;130:484–90.
[49] Monthly Electricity Trading Report, Electricity and Gas Market Surveillance Commission. Available at: https://www.emsc.meti.go.jp/info/business/report/results.html.
[50] Turton R, Bailie RC, Whiting WB, Shaeiwitz JA. Analysis, synthesis, and design of chemical processes, 3rded.. Pearson Education; 2008.